

Two-dimensional MHD models of solar magnetogranulation. Dynamics of magnetic elements

V.A. Sheminova

Main Astronomical Observatory, National Academy of Sciences of Ukraine
Zabolotnoho 27, 03689 Kyiv, Ukraine
E-mail: shem@mao.kiev.ua

Abstract

We present the results of a statistical analysis of the Doppler shifts and the asymmetry parameters of V profiles of the Fe I 630.25 nm line produced by 2D MHD simulations of solar granulation. The realism of the simulations tested using the magnetic ratio of Fe I 524.71 and 525.02 nm lines. The Stokes spectra were synthesized in snapshots with a mixed polarity field having a mean magnetic flux density of 0.2 mT and mean unsigned field strength of 35 mT. We found that downflows with a velocity of 0.5 km s^{-1} predominate, on the average, in areas with some network magnetic elements at the disk center. In separate strong fluxtubes average velocity is equal to 3 km s^{-1} and the maximum velocity is 9 km s^{-1} . In weak diffuse magnetic fields upflows dominate. Their average velocity is 0.5 km s^{-1} and maximal one is 3 km s^{-1} . The V -profile asymmetry depends on the spatial resolution. The V profiles synthesized with high spatial resolution (35 km) have average amplitude and area asymmetries -1% , 1% , respectively. The asymmetry scatter is $\pm 70\%$ for weak profiles and $\pm 10\%$ for strong ones. The profiles with low spatial resolution (700 km) have average amplitude and area asymmetries 3% , -2% , respectively. Low spatial resolution is a reason why the amplitude asymmetry is always positive and greater than the area asymmetry in V profiles observed. We found weak correlation between the asymmetry of V profiles and velocity. Upflows cause negative asymmetry, on the average, and downflows cause positive asymmetry. We examined center-to-limb variations of vertical velocity in magnetic elements. Beginning from $\cos \theta = 0.9$, the average velocity abruptly increases from 0.5 to 2 km s^{-1} and then slightly varies closer to the limb. We found nonlinear oscillations of vertical velocity with power peaks in the 5-minute and 3-minute bands. This nonlinearity is caused by magnetic field strength fluctuations in fluxtubes. The Doppler shifts and asymmetry parameters obtained for space-average V profiles are consistent with results of FTS observations as well as with other observations made with higher spatial resolution.

1 Introduction

Magnetic fields on the Sun exhibit fine structure which is conditioned by the fine structure of the solar surface in general and its active regions in particular [30]. The first supporting evidence for the fine structure of magnetic fields was found in the 1960s, initially in strong fields in spots and later in quiet regions [30]. Magnetic fields outside spots were found to be

unevenly distributed over the surface, in the form of dense magnetic fluxes in very small areas ($\approx 1''$). Kilogauss strengths of these compact magnetic features were initially measured in faculae and in the supergranular network by the line-ratio method [16, 44, 46]. These results were confirmed more than once in later studies. According to [44], the typical size of magnetic concentrations is 100–300 km, typical strength is 100–200 mT, the velocity does not exceed 1.2 km s^{-1} and is 0.5 km s^{-1} on the average. The field strength scatter is very small. The authors of [16] concluded that 90 percent of the photospheric magnetic field is concentrated in compact kilogauss structures and 10 percent is found in quiet regions with a mean flux density of 0.2–0.3 mT. Further investigations revealed that fine compact magnetic features have a filamentary structure and look like tubes with their diameter growing with height in the atmosphere (the mushroom or canopy effect). They are tilted most probably at an angle of 10° [11, 24]. The temperature in them is higher in the middle and upper photosphere and is lower in the lower photosphere as compared to the quiet Sun, and the chromospheric temperature growth begins in deeper layers as compared to the quiet Sun [38]. Analyses of all available data revealed a wonderful property of these magnetic structures — despite some distinctions in size, field strength, and orientation, they all are much alike in form and in their magnetic and temperature properties. Because of this, they were pooled to form a separate class of solar magnetic structures and were called the small-scale magnetic elements or magnetic flux tubes [29, 38]. The number of flux tubes on the solar surface increases with decreasing tube size. Although each magnetic element adds very little to the general solar radiation flux, millions of magnetic elements not only compensate for the energy blocked in spots but even produce some additional radiation (about 0.1 percent [39]). Magnetic flux tubes can form clusters of various sizes. These clusters are assumed to form larger magnetic structures such as the active supergranular network, faculae, and plages. At present the smallest (120 km) magnetic elements resolved in observations are the so-called bright points of magnetic network [4].

Concurrent with the refinement of observation techniques, theoretical models of magnetoconvection in quiet regions on the Sun have been developed. Much research was devoted to numerical simulation of magnetic elements, their formation and interaction with convective motions (see review [29]).

In this study we use two-dimensional MHD models developed by Gadun [6, 9, 25]. Unlike other researchers, he used an original approach to the solution of the equations of radiation magnetohydrodynamics [7] which describe a compressible, gravitationally stratified turbulent medium. The magnetic field is described by the vector potential, so that the divergence of magnetic field strength is always zero in the simulation region. The initial magnetic field is specified by a bipolar magnetic configuration. The first sequence of 2D MHD models [6] of completely nonstationary solar magnetogranulation extended over a long time period (two hours of solar time). With such models, the evolution of solar magnetic elements, their structure and dynamics could be studied in detail on scales much smaller than the spatial resolution of the present-day observations. Three-dimensional models (e.g., [41]) are certain to give more realistic flow patterns, while two-dimensional models more adequately represent small-scale phenomena, and they still remain useful in studying the properties of magnetic elements. Analyses of 2D simulations of convection [8, 27] and magnetoconvection [2, 3, 13, 43] suggest that 2D models reproduce quite well many features of 3-D convection. The major results of 2D magnetoconvection simulations on granulation scales obtained by Gadun were presented in [6]. Investigations into the mechanism of formation and destruction of flux tubes and into their stability conditions revealed that thermal flows are the most important factor in the evolution of small-scale magnetic fields. Fragmentation of large-scale thermal flows can result in the formation of vertical magnetic elements from horizontal magnetic surface flows. This previously unknown mechanism of flux tube formation was called the surface mechanism [7, 9]. The mechanism of

formation of kilogauss flux tubes through convection collapse was also investigated, and some spectropolarimetric manifestations of this process were found [35]. MHD models [6] pointed to the emergence, reconnection, and recycling of magnetic flux near the surface, and these processes were demonstrated in [26]. Nonstationary MHD models [6] can serve as an analog of some observed photospheric regions with average unsigned strength of magnetic fields of 40–50 mT. These heterogeneous models, which are more realistic than two-component models, were also used to calculate the Stokes profiles of photospheric lines [32, 34, 26]. In particular, the analysis of the V profiles of the IR line Fe I λ 1564.8 nm [34] gave a magnetic field intensity distribution which is in good agreement with observations of magnetic fields in quiet regions [19] and which confirms the two-component structure of intra-network fields.

The magnetic field in the solar plasma is closely associated with the velocity field, and this association inside sunspots as well as in the quiet solar atmosphere still is one of the most difficult problems in solar physics. The freezing of magnetic field in the moving plasma (or its rigid connection with velocity field) can be weakened due to the fine structure of this magnetic field [30]. That is why the study of dynamic processes in magnetic elements, and inside strong flux tubes in particular, by the magnetoconvection simulation techniques is of current interest, inasmuch as the magnetic elements still are not spatially resolved because of their small horizontal size. Numerical MHD simulations [2, 43] suggested that a large variety of dynamic processes should be expected on scales of several hundred kilometers inside and outside flux tubes. Recent highly accurate polarimetric observations in the line Fe I λ 630.25 nm with a spatial resolution better than 700 km [36] yielded some statistical relations between the observed Stokes V -profile parameters which are indicative of substantial systematic motions in the magnetic elements in the network, faculae, and quiet regions. We believe that the reproduction of some observed spectropolarimetric effects [20, 24, 36] with the use of 2D MHD models [6] is of obvious interest.

The main purpose of this study is to determine the dynamical characteristics of magnetic elements in the solar photosphere. Below we give some principal results of observations of the magnetic element dynamics, a description of the 2D MHD models we use, and the results of the application of the line-ratio method to these models. We also analyze our calculations of the Stokes V profiles, their shifts, asymmetries, and center-to-limb variations on scales smaller than or comparable to the spatial resolution of present-day observations.

2 Observed shifts and asymmetries of V profiles

Studies based on complex magnetographic observations of magnetic fields and line-of-sight velocities revealed that the vertical velocities are equal to zero, on the average, at the chromospheric network boundaries as well as inside network cells [50], while the line-of-sight velocities determined from spectropolarimetric observations were contradictory [29]. Early extensive polarimetric observations with Fourier spectrometers (FTS) with high spectral resolution and low spatial and time resolutions (about $10''$ and 30 min) detected no significant systematic motions (above 0.25 km s^{-1}) inside flux tubes [40]. This result differed essentially from a mean velocity of 0.5 km s^{-1} derived earlier in [44]. Only observations with high spatial resolution ($\approx 1''$) [32] detected a small predominance of downflows with a mean velocity of 0.2 km s^{-1} and the dependence of this velocity on the size of magnetic elements. In regions with small filling factor, downflows were stronger and the velocity scatter increased from -0.5 km s^{-1} to 1.5 km s^{-1} . The mean velocity measured in [11] was about 0.8 km s^{-1} , and the scatter increased with decreasing amount of polarization. Theoretical simulations of the interaction between convection and magnetic field [2, 13] also confirmed the existence of systematic motions outside and inside

flux tubes on small spatial and temporal scales. A most impressive evidence that dynamic processes are stronger inside magnetic elements was given in recent studies [19, 36]. Systematic downward motions observed with a spatial resolution of 0.8–1'' were found to have mean velocities of 0.5–0.7 km s⁻¹. In magnetic elements with small filling factor the velocities were as high as ±5 km s⁻¹, while they were smaller in elements with large filling factor or in clusters. Some evidence for large horizontal velocities of about 2 km s⁻¹ in magnetic elements was given in [51].

In addition to the zero-crossing Doppler shifts, the asymmetry of observed V profiles is used for the diagnostics of motions in flux tubes. This asymmetry detected for the first time in [37] from FTS observations near the disk center was “blue”, i.e., the amplitude and area of the shortwave peak were greater, on the average, than in the longwave peak, the amplitude asymmetry being several fold greater than the area asymmetry. The general trends found in [37] have been confirmed by observations made with various resolutions, but the asymmetry magnitude slightly decreased with growing resolution. Numerous investigations demonstrated that the V profiles owe their asymmetry to the combined effect of the magnetic field and velocity field gradients inside flux tubes and around them [29]. A large number of profiles with extremely large asymmetries were recently found in observations with resolutions below 700 km. For example, three percent of all Fe I λ 630.25 nm line profiles observed in the network regions and in faculae have such asymmetries [36]. Atypical V profiles, especially those which have one wing only, are of special interest. They were shown in MHD simulations to appear mainly at the periphery of magnetic elements [26]. Extremely large asymmetry can be caused by strong downflows below the canopy near flux tube boundaries.

So, polarimetric observations with high spatial resolutions demonstrated that the dynamical characteristics of magnetic elements have a much wider range than that assumed before. What can we expect from observations in which the structure of magnetic elements will be resolved? We tackled this question with the use of the results of the 2D MHD simulation of magnetic elements and the synthesis of the Stokes profiles of the Fe I λ 630.25 nm line.

3 Two-dimensional MHD models

The sequence of MHD models we use here was described in detail in [6, 7, 9]. The simulated region 3920×1820 km in size had 112 vertical columns (rays) with a 35-km spatial step. The starting magnetic field had bipolar decreasing with growing height, the mean unsigned field strength was 5.4 mT. The magnetic field was evolving in the course of two-hour simulation, and its unsigned strength grew to 50 mT on the average. Strong flux tubes are formed after a lapse of 50 min of simulation. They disintegrate and form again in the simulation region. In one of the snapshots displayed in Fig. 1 two kilogauss flux tubes of different polarities can be seen to approach each other and to destroy one the other a short time later. The horizontal size of flux tubes at the level of visible surface ($\log \tau = 0$) varies from 35 km to 350 km in the course of evolution, and the maximum strength of their fields varies correspondingly from 40 mT to 250 mT. The largest area (about 50 percent) is occupied throughout the simulation time by flux tubes with diameters of 80–180 km and field strengths of 100–200 mT [6].

Our study is based on a sequence of the snapshots of half an hour’s duration after 94 minutes of simulation with a 30-s step. This is a period when strong flux tubes are intensely evolving. Two flux tubes of opposite polarities are often formed in the simulation region. As a rule, flux tubes are accompanied by nearby weak fields of opposite polarity. In upper lateral layers of flux tubes hot regions appear as a result of deceleration of strong granulation flows near the tube walls. These hot regions may be analogs of observed bright points [4].

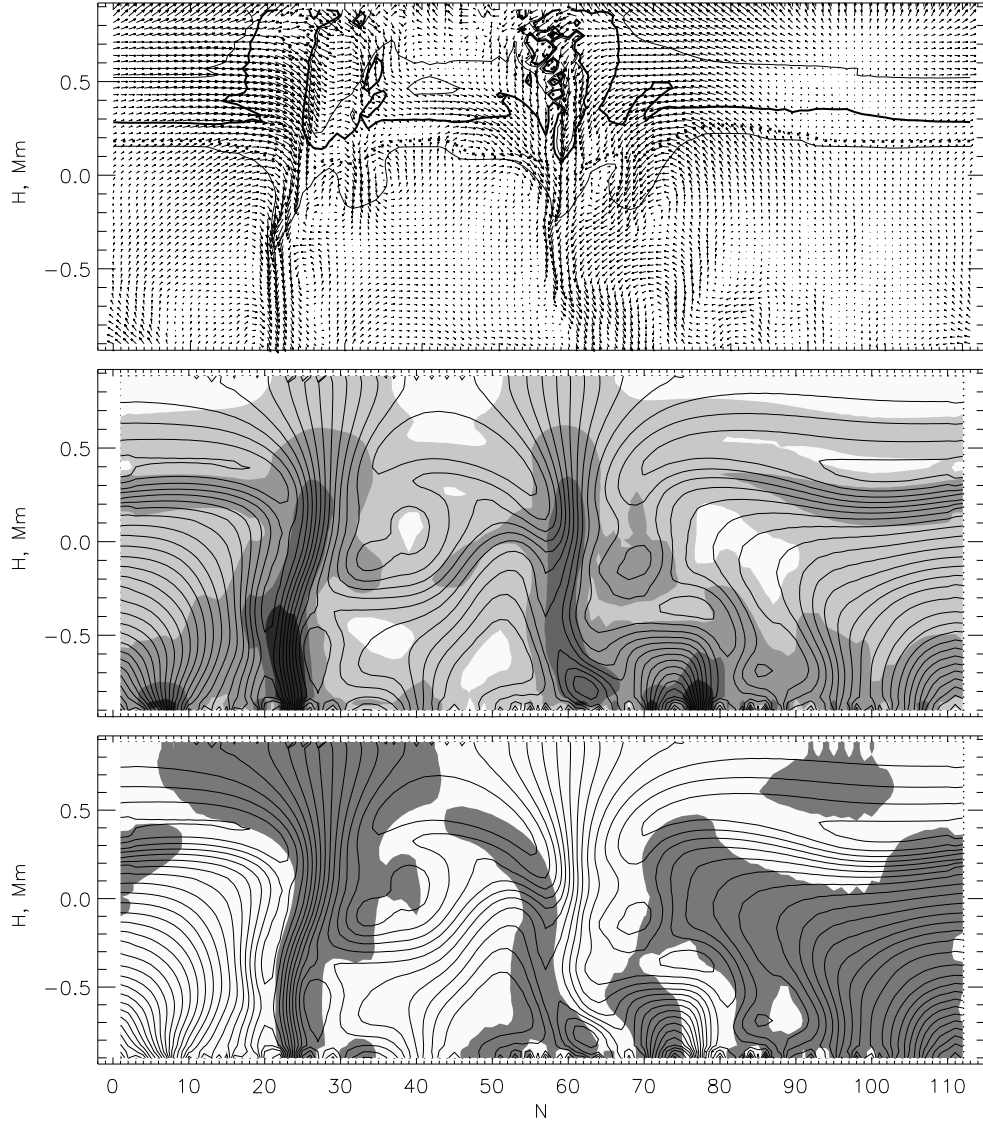


Figure 1: A snapshot from 2D MHD simulation [6] at moment 95.5 min: a) velocity field (arrow length is proportional to velocity magnitude) and isotherms (from top to bottom) corresponding to 4000 K (thin line), 5000 K (thick line), 6500 K (dotted line), and 10000 K (thin line); b) field lines and magnetic field strength (shading density is proportional to field strengths of 1, 20, 50, 100, 150 mT); c) field lines and field polarity (grey area shows positive polarity and white area negative polarity). Vertical axis) geometric height H , horizontal axis) column number N in the MHD model; distance between the columns is 35 km.

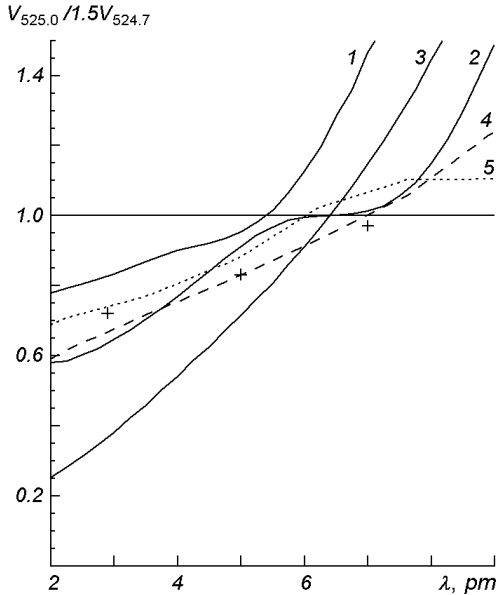


Figure 2: Ratio of V profiles of Fe I lines $\lambda\lambda$ 525.0 and 524.7 nm as a function of the distance from V -profile center. Solid curves were obtained from MHD models: 1) for region with one subkilogauss flux tube, 2) for region with two kilogauss flux tubes, 3) for axis of kilogauss flux tube; plusses) observations [28] outside active regions; curve 4) observations [46] for strong faculae; curve 5) observations [46] for weak faculae.

Predominantly horizontal magnetic fields are observed in the central parts of granular cells. All these peculiarities of the simulated magnetogranulation can be seen in the vertical section of the simulation region (Fig. 1). We assume that the selected snapshots sequence represents the quiet Sun regions with some network elements because the unsigned field strength distribution mode is 35 mT in the simulation region and the flux density is 0.2 mT [34].

4 Testing the MHD models

The MHD models we use were tested in [32]. Here we continue to test them by the method of field strength ratio measured in two spectral lines [44]. This well-known method was widely used for the diagnostics of strong magnetic fields outside active regions on the Sun in low spatial resolution spectra (1–4'') [10, 16, 17, 46], and now it is applied to high-resolution spectra (< 1'') [17, 52]. The effectivity of the line-ratio method depends on the model atmosphere chosen for the field strength calibration, so that the method also needs testing with models which are more realistic than the two-component models commonly used for calibration [17]. Applying this method to MHD models, we can test the models and the method itself.

As in observations, we chose two Fe I lines – $\lambda\lambda$ 524.71 and 525.02 nm. Their atomic parameters are nearly the same, and only the Lande factors differ (their ratio is 1.5). Therefore, the ratios of calibrated magnetograph signals in two lines – $B_{525.0}/B_{524.7}$ or $V_{525.0}/(1.5V_{524.7})$ – should be insensitive to all atmospheric parameters except field strength, magnetic field inclination, and velocity field. As shown in [28, 45, 46], the “magnetic ratio” also depends on the position of the selected V -profile section with respect to the profile center – as the magnetograph slit approaches the line center, the ratio decreases. The line ratio also depends on the filling factor in the resolved area and on lateral magnetic field profile. Thus, the magnetic field strength found by the line-ratio method depends on the spatial and spectral resolutions of observed spectra.

We determined the ratio of V signals as a function of distance to line center $MLR(\Delta\lambda) = V_{525.0}(\Delta\lambda)/[1.5V_{524.7}(\Delta\lambda)]$ for the profiles in different simulation regions. The Doppler shifts of V profiles with respect to the central wavelength of I profiles were compensated. Figure 2 illustrates three $MLR(\Delta\lambda)$ relations. One relation was derived from profiles averaged over a 3'' region with a relatively weak subkilogauss flux tube ($B_0 \leq 90$ mT), the second relation refers to

an area of the same size with two strong flux tubes with $B_0 \leq 190$ mT, and the third relation is based on the profiles corresponding to the axis of a strong flux tube with $B_0 \geq 180$ mT at the level $\log \tau_5 = 0$ (without spatial averaging). We also plotted the relations for the ratios $B_{525.0}/B_{524.7}$ (observations from [28]) and $V_{525.0}(\Delta\lambda)/[1.5V_{524.7}(\Delta\lambda)]$ (FTS observations of regions with strong and weak faculae [47]). The magnetic ratio is greater at greater distances from line center and is greater than unity in distant line wings. At lower resolutions, the relation is less steep and the magnetic ratio is smaller (cf curves 2 and 3). The run of relation 2 (the region with two strong flux tubes and with low resolution) is in good agreement with observation data, and this supports our earlier inference [32] that the theoretical MHD models [6] represent quite well the actual magnetic fields on the Sun.

The run of the $MLR(\Delta\lambda)$ relations derived for different magnetic fluxes from MHD models is the same as the run derived earlier with the use of two-component models [28, 45]. These relations roughly represent various cases of magnetic saturation and various long-wave shifts of V signals in different sections of the profiles of two lines. Kilogauss fields not only diminish the V -profile amplitude but substantially change the profile shape as well. In strong fields the $V_{525.0}$ profile is lower and wider than the $V_{524.7}$ profile, and the ratio of magnetic saturations in two lines becomes reverse at a distance of 5–7 pm from the line centers: MLR becomes greater than unity. So, the $MLR(\Delta\lambda)$ relations we derived clearly demonstrate that the magnetic fields measured by the line-ratio method heavily depend on the line section ($\Delta\lambda$) chosen for the measurements.

The ratio of V -profile amplitudes $MLR = a_{V,525.0}/(1.5a_{V,524.7})$, which is independent of $\Delta\lambda$, is sometimes used in polarimetric observations [46]. We determined the amplitude ratio for 5824 V profiles calculated in every MHD model column (Fig. 3a). There is a correlation between the “magnetic ratio” and the amplitude $a_{V,525.0}$: the ratio decreases, on the average, with increasing V -profile amplitude, and this suggest that the magnetic field increases. We also determined MLR for profiles averaged with a 1'' resolution. This spatial averaging markedly affected the V -profile amplitudes and consequently the magnetic ratio (Fig. 3b); the MLR scatter increased in every interval and the correlation between MLR and profile amplitude deteriorated. The number of atypically shaped profiles (with one wing or with several wings) was found to grow among weaker V profiles, and this can affect the accuracy with which mean V -profile amplitudes are calculated. It should be noted that the Fe I lines $\lambda\lambda$ 524.71 and 525.02 nm have very narrow profiles which are highly sensitive to temperature, so that the effect of extreme asymmetry of weak V profiles is stronger for these lines, and this accounts for the greater scatter in MLR for small V -profile amplitudes.

We calculated the MLR values in order to transform the magnetic ratios into field strengths. This was done with the data for the MHD model shown in Fig. 1. We calculated MLR and effective heights of V -profile peak formation for each model column. Having found the level at which the method locates the magnetic field, we determined the field strength for this level directly from the model and plotted the MLR – B relation (Fig. 3c). We found from this relation that a decrease of MLR from 0.94 to 0.82 (Fig. 3a) corresponds to a growth of B from 30 to 62 mT (Fig. 3c). This means that, according to the line-ratio method, the field strength in the simulation region can be 60 ± 30 mT at the most, i.e., the method did not fix any strong fields about 150 mT appropriate for the MHD models we use. The averaged magnetic line ratio is 0.88 ± 0.10 , and the corresponding mean field strength in the simulation region is 43 mT, in good agreement with the simulation results for our MHD model sequence (40–50 mT) and with the results obtained in [52] by the line-ratio method applied to the V profiles of the same two lines observed in quiet regions with high spatial resolution. No significant deviations of MLR from unity were found in [52], and the intra-network fields were concluded to have no kilogauss structures; the typical field strength was estimated at 20–50 mT. The coincidence of the data

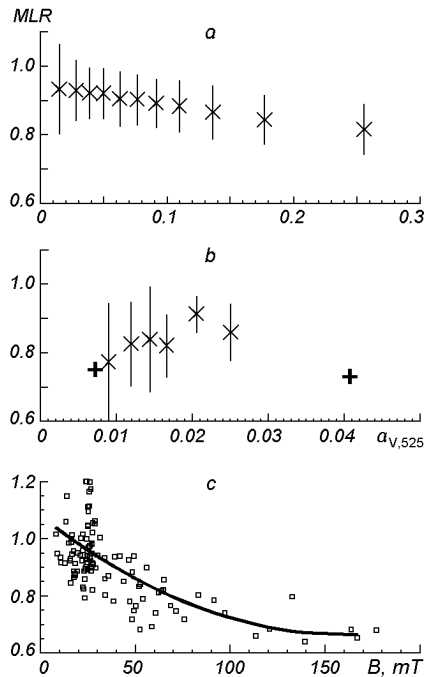


Figure 3: Magnetic ratio $MLR = a_{V,525.0}/(1.5a_{V,524.7})$: a) without averaging, b) with spatial averaging over 700 km. Standard deviations are shown for some intervals with the same number of points; c) dependence of MLR on magnetic field strength B derived from the data of the snapshot shown in Fig. 1.

from [52] with the mean field strength in the MHD models we used allows us to suggest that our simulation region is similar to quiet solar regions.

Thus, the testing of MHD models by the line-ratio method with the use of the Fe I lines $\lambda\lambda$ 524.71 and 525.02 nm showed a satisfactory agreement between the calculated and observed magnetic ratios as functions of the distance from the V -profile center. This suggests that the MHD models [6] describe adequately the fine structure of actual magnetic fields of the quiet Sun. The testing also demonstrated that fields stronger than 100 mT with filling factors of 1–5 percent cannot be detected by the line-ratio method in quiet regions on the Sun, since this method depends on spatial resolution. Nevertheless, the method can give a reliable estimate for the mean field strength in quiet regions.

5 Results of analysis of synthesized V profiles

The Stokes profiles of the Fe I line λ 630.25 nm were calculated for every column in the MHD models by integrating the Unno-Rachkovskii equations for the polarized radiation transfer in the LTE approximation [31]. We chose this moderately strong photospheric line for the V -profile analysis because it is most often used, together with the Fe I line λ 630.15 nm, in polarimetric measurements [1, 20, 22, 23, 36]. A telluric O_2 line which is observed in the I -profile wing does not affect the V profile. The line λ 630.25 nm is preferred to the magnetic Fe I lines $\lambda\lambda$ 524.7 and 520.5 nm not only because of its unblended V profile but also due to its high sensitivity to magnetic field and much smaller sensitivity to temperature irregularities. The V profile of Fe I λ 630.25 nm is formed rather deep in the photosphere, at the level $\log \tau_5 = -1$, on the average, and thus it can be calculated in the LTE approximation. It should be stressed that the dynamical characteristics of magnetic elements studied with the use of this line refer to the same photospheric level. This is particularly true for the velocity and magnetic field gradients which can suddenly change in highly inhomogeneous media, for example, at the periphery of compact magnetic features. That is why the asymmetry magnitude and sign, which attest to the existence of gradients, as well as the relationship between the asymmetry and other parameters found in our study can differ from the results obtained with the use of other lines.

We compared our calculations to the FTS observation data kindly made available by J. Stenflo and S. Solanki. These observations were made in quiet network elements and in active facula regions at the McMath telescope in 1979; the Fourier spectrograph had a high spectral resolution (420 000) and low spatial and time resolutions (10'' and 35–52 min, respectively) [47]. We used only the V profiles of Fe I and Fe II lines in the wavelength range from 445.0 to 557.0 nm. The observed V profile parameters were calculated by Solanki's codes, and the absolute zero-crossing shifts were determined by the method proposed in [5].

We analyzed the following V -profile parameters. 1. Mean amplitude of blue (b) and red (r) wings $a_V = (|a_b| + |a_r|)/2$. 2. Doppler zero-crossing shift with respect to the absolute wavelength (transformed into the line-of-sight velocity V_z by the standard formula). 3. Amplitude asymmetry $\delta a = (|a_b| - |a_r|)/(|a_b| + |a_r|)$ and area asymmetry $\delta A = |A_b| - |A_r|/(|A_b| + |A_r|)$. The blue and red wing amplitudes (a_b and a_r) and the zero-crossing position were calculated by fitting the corresponding profile sections to polynomials. The areas A_b and A_r were obtained by integrating the V/I_c profile from zero-crossing to a 0.5-percent level in the red and blue wings.

By analogy with the observation data from [36], we used only the profiles with amplitudes greater than 0.15 percent and regularly shaped profiles, i.e., only those with two wings of different signs and with one zero-crossing. The number of such profiles was 3755; the rest were either very weak or abnormal in shape (symmetric, with one wing only, or with several zero-crossings), and they were excluded from the analysis.

Mean V -profile amplitudes. Figure 4 (upper part) demonstrates the a_V distribution obtained from V -profiles calculated without spatial averaging and with a 1'' averaging. When the histogram for all profiles is compared to the histogram for regularly shaped profiles (without strong anomalies), one can see that weak profiles are less numerous in the second case due to highly asymmetry of weak profiles. Spatial averaging of profiles essentially changes their distribution. Recall that the maximum diameter of simulated flux tubes is about 350 km, so that the profiles averaged over a 700-km area do not resolve the tube structure, and profiles with amplitudes above 10 percent are absent in the histogram.

In the analyses of observed Stokes profiles, a_V is most often used as a substitute for filling factor or as an indicator of the longitudinal magnetic field. The statistical relations for a_V shown in Fig. 4 (lower part) were averaged over the intervals of the field strength B and field inclination γ , they were obtained directly from the MHD models for the optical depth $\log \tau_5 = -1$ and from the continuum intensity contrast $I_c / \langle I_c \rangle$. Here I_c is the continuum intensity calculated for a specific model column and $\langle I_c \rangle$ is the intensity averaged over the entire simulation region in the model. There is a close correlation between B and a_V as well as between γ and a_V . The relationship between $I_c / \langle I_c \rangle$ and a_V is more complicated — the weakest V -profiles correspond to high-contrast areas, the strongest profiles correspond to low-contrast areas, while moderately strong profiles represent areas with slightly changing contrast.

So, the nearly linear a_V – B relation found suggests that a_V can be used as a magnetic field indicator in the analyses of Stokes profiles.

Zero-crossing shifts. The line-of-sight velocities (V_z) of the magnetized plasmas flows only are derived from the Doppler shifts of V profiles or the so-called zero-crossing shifts. Positive (red) shifts point to downflows and negative (blue) shifts to upflows. Figure 5 (upper part) displays the Doppler shifts converted into V_z as functions of three principal parameters derived usually from the observed V -profiles: a_V (indicator of magnetic field strength), magnetic vector inclination γ , and intensity contrast $I_c / \langle I_c \rangle$. The inclination angle was derived from the amplitude ratio for Stokes profiles: $\tan^2 \gamma \approx Q^2 + U^2 / V^2$.

The distribution of V_z s (Fig. 5, left) points to a well-marked asymmetry between upflows and downflows – a fundamental property of magnetoconvection in a matter with frozen magnetic

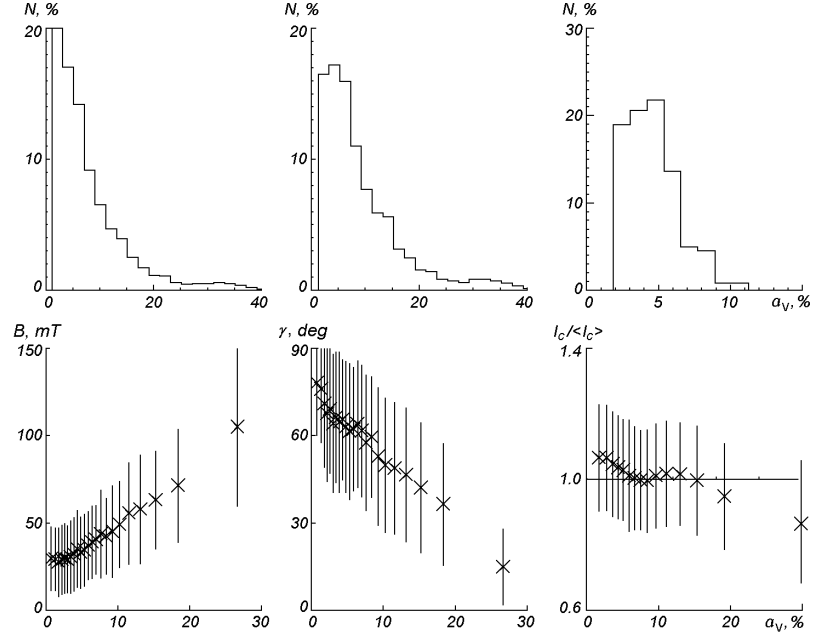


Figure 4: Upper plots) distributions of V profile amplitudes a_V from 52 MHD snapshots: at the left) for all 5824 profiles ($\bar{a}_V = 7\%$); at the center) with abnormal profiles excluded (3755 profiles, $\bar{a}_V = 9\%$); at the right) for profiles spatially averaged with a 700-km step (243 profiles, $\bar{a}_V = 4\%$). Lower plots) unsigned field strength, field inclination angle, and contrast of continuum intensity as functions of amplitude a_V .

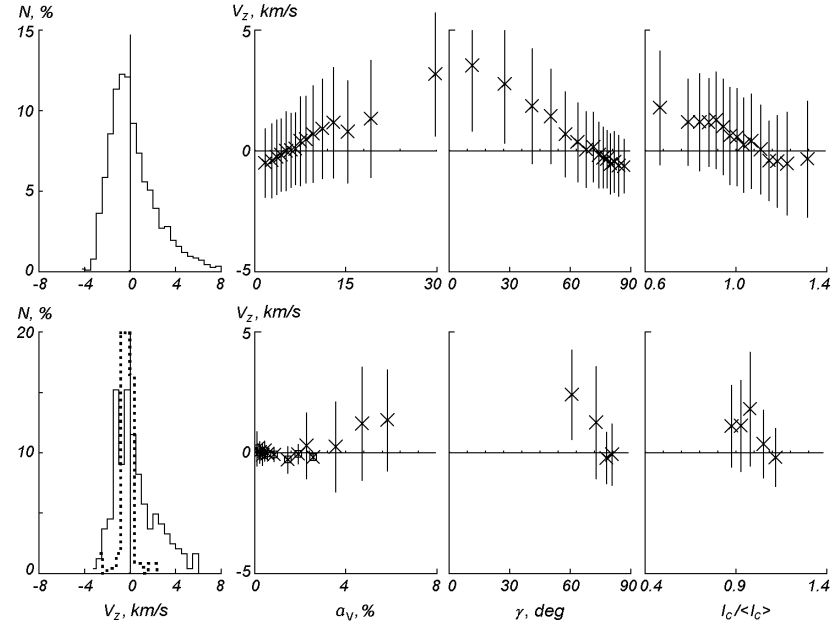


Figure 5: V_z histograms derived from the zero-crossing shifts of V profiles, and the V_z dependence on a_V , γ , and $I_c / \langle I_c \rangle$: upper plots) all profiles, lower plots) profiles averaged with a 700-km step. Dotted line and squares) FTS observation data.

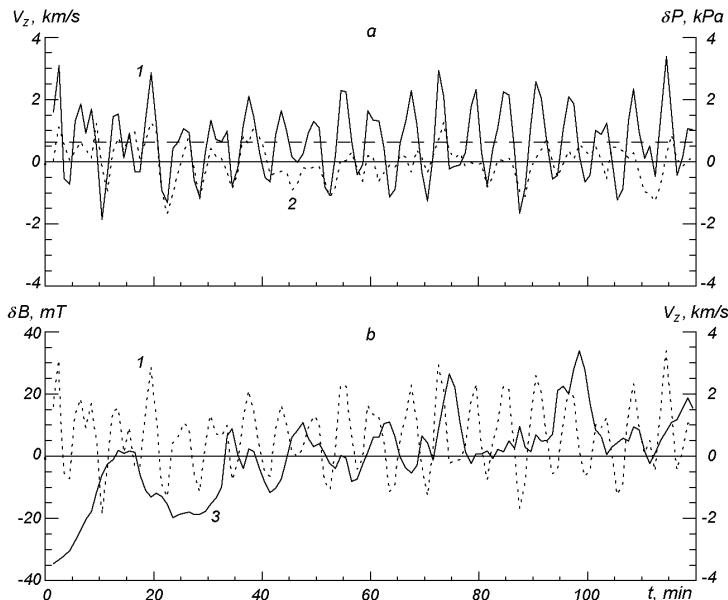


Figure 6: Oscillations derived from 2D MHD model of solar granulation. a) Vertical velocity V_z (curve 1), gas pressure fluctuations δP (curve 2). Dashed straight line) mean velocity of 0.6 ± 1.1 km s $^{-1}$. b) V_z (curve 1), unsigned magnetic field strength δB at the level $\log \tau_5 = 0$ (curve 3). V_z , δP , and δB are averaged over whole simulation region.

field. The velocity distribution maximum lies at -1 km s $^{-1}$ approximately. A mean velocity of 0.53 km s $^{-1}$ and a wide velocity range from -3 km s $^{-1}$ to 9 km s $^{-1}$ suggest that downflows dominate in the magnetized plasma. There is a correlation between velocity and principal parameters of V profiles. The downflow (positive) velocity increases to 3 km s $^{-1}$, on the average, with increasing a_V (B), with decreasing γ and $I_c / \langle I_c \rangle$, and this suggests that the most rapidly moving plasma resides in strong (120 mT) nearly vertical (10°) flux tubes with low contrast (0.7), which corresponds to darker intergranular lanes. The above correlations are in accord with the physical properties of convective motions which affects the distribution of LOS velocities and magnetic fields in photosphere (see velocity field of the convective motions in the snapshot, Fig. 1).

The spatial averaging of profiles decreases the fraction of very weak profiles with negative velocities and very strong profiles with high positive velocities (the lower part of Fig. 5). The spatial averaging increased the mean value of V_z to 0.72 km s $^{-1}$. All relations in the lower part of Fig. 5 preserved the trends pronounced in the upper plots.

Our results agree satisfactorily with the observations of magnetic regions outside activity centers analyzed in [36], where the mean velocity was estimated at 0.73 km s $^{-1}$ and the velocities ranged from -6 to 6 km s $^{-1}$. In [19] \overline{V}_z was 0.25 km s $^{-1}$ and the range was from -3 to 5 km s $^{-1}$. We also plotted the FTS observation data from [47] ($\overline{V}_z = -0.04$ km s $^{-1}$) in Fig. 5. Our results are in good agreement with observed velocities in the regions of small a_V .

Oscillations. Although wave processes in spatially unresolved flux tubes are difficult to detect directly, oscillatory motions with a 5-minute period along flux tubes have been reported [38]. There is also some evidence for oscillations with a shorter period [51]. Observations with high spatial resolutions [1] revealed velocity oscillations with an amplitude of about 1 km s $^{-1}$. Theory predicts a wide variety of wave modes in solar flux tubes and their importance in the heating of the chromosphere and corona. According to the 2D MHD simulation [6] velocities of vertical flows in magnetized plasmas can vary in a wide range (see Fig. 5). It points to an oscillatory instability of magnetogranulation regions. Here we examined the temporal changes of velocity V_z derived from shifts of V profiles averaged over in the whole simulation region for the complete two-hour sequence of MHD models with a 1-minute interval. Fig. 6a shows obtained vertical velocities as functions of time. We also calculated the power spectrum of velocity oscillations (Fig. 7a), where two power peaks can be clearly seen in the bands at 5 min

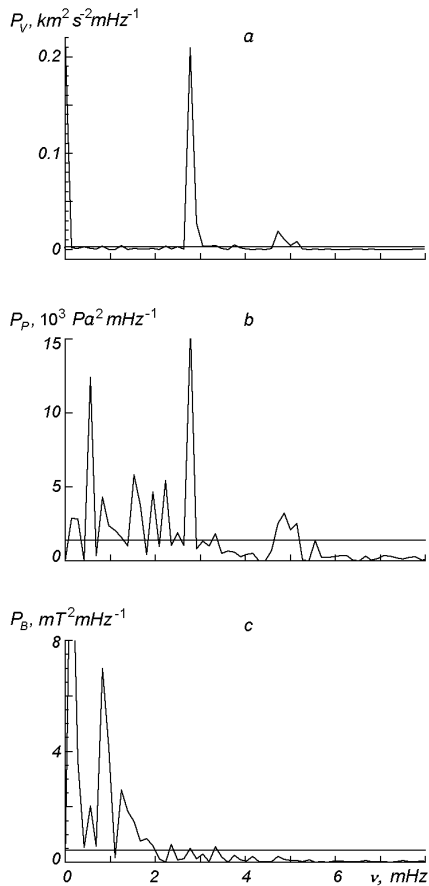


Figure 7: Power spectra of vertical velocity V_z oscillations (a), gas pressure fluctuations δ_P (b), and field strength fluctuations δ_B at the level $\log \tau_5 = 0$ (c). Straight line) 99-percent confidence level determined in accordance with [14].

($2 < \nu < 4.5$ mHz) and 3 min ($4.5 < \nu < 7$ mHz). The power maximum lies at $\nu \approx 2.8$ mHz (5.9 min), and a smaller peak lies at $\nu \approx 4.7$ mHz (3.5 min). A 99-percent confidence level shown by a horizontal line in the figure was calculated in accordance with [14] from the mean power in the band 5.5–8.3 mHz. The Nyquist frequency is equal to 8.3 mHz.

Velocity oscillations with frequencies of 2.57, 3.88, and 5.58 mHz were also obtained in [42] from a 3-D simulation of the solar surface convection in the absence of magnetic field. The p-mode oscillations were assumed to be excited by random nonadiabatic pressure fluctuations near the Sun’s surface. Such fluctuations are produced by the radiative cooling which can locally deviate for a short time from equilibrium with the heating produced by convective motions. Figure 6a shows the gas pressure fluctuations δP_g calculated for our models. Here P_g is the pressure averaged over one model at a specific point in time and $\langle P_g \rangle$ is the pressure averaged over all models in a time interval of 120 min. Comparison of the velocity and pressure oscillations suggests that there should be a relationship between them. In the power spectrum calculated for pressure oscillations (Fig. 7b) there are power peaks at the same frequencies as in the spectrum of velocity oscillations in the 5-min and 3-min bands.

To examine the influence of magnetic field on the oscillations of vertical velocities, we obtained the field strength fluctuations δB (Fig. 6b) from the simulation data and calculated their power spectrum (Fig. 7c). First of all we point out a constant increase of the magnetic field and its well-marked oscillations associated with the evolution and disruption of strong flux tubes in the simulation region. A strong peak in the field strength oscillation power was found at $\nu = 0.83$ mHz (20 min) and a smaller peak was found at 1.25 mHz (13 min). When comparing the magnetic field oscillations with vertical velocity oscillations, we found that the negative velocity component almost disappeared and the positive component increased when the magnetic field was stronger, that is, the upflows were slower and downflows faster. This

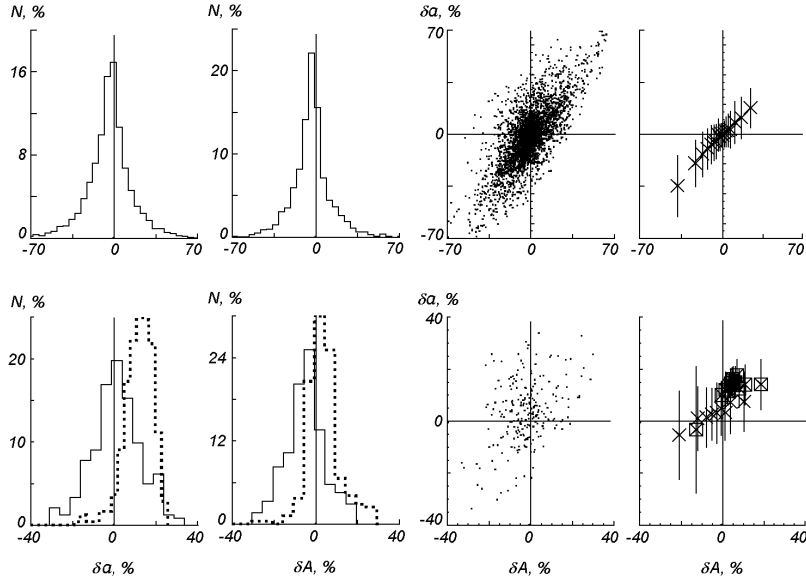


Figure 8: Distributions of amplitude asymmetry δa and area asymmetry δA of V profiles, scatter of asymmetry parameters and their correlations: upper plots) all profiles, lower plots) profiles averaged with a 700-km step. Dotted line and square) FTS observation data.

means that the velocity oscillations are nonlinear. Such quasi-oscillatory motions in flux tubes were predicted in [12]. Nonlinear oscillations were considered there to be a superposition of upflows and downflows with different amplitudes and durations. The upflow velocities were estimated there at -0.5 km s^{-1} and downflow velocities at about 2 km s^{-1} . Our results for the moments of magnetic field strengthening are very close to these data. As seen in Fig. 6a, the magnetic field modulates the velocity oscillations. Based on the results of MHD simulation [6], we attribute this effect to convective instability in intergranular lanes. About 10–12 min after the formation of a strong flux tube begins, conditions favorable for convective collapse set up, and the collapse produces a kilogauss field. Then the flux tube is in a quasi-stable state for some time ($\leq 10 \text{ min}$), it is narrower and closer to the vertical, its temperature grows, the field is stronger, and the Wilson depression correlates with the vertical velocity. Oscillatory downward motions become more intense in the flux tube region. After each abrupt downward shift of magnetic configuration, there comes a period of a slacker convective collapse. These oscillations persist until the strong evacuation in the upper part of the flux tube begins to destroy the tube (i.e., until the beginning of reverse convective collapse). As this takes place, downflows are replaced by upflows with supersonic velocities. The flux tube rapidly dissipates in the course of several minutes. The size and the inclination of the flux tube increase, the magnetic field and the temperature diminish, the Wilson depression also diminishes. As the dynamical condition changes, the inclination of flux tubes also changes with time — it oscillates. This can give rise to waves propagating along the flux tubes [43].

So, the convective and superconvective instability processes going in strong flux tubes bring about a nonlinearity in the oscillatory motions of magnetized plasmas in the simulation region.

Asymmetry. Figure 8 demonstrates the distribution of the amplitude and area asymmetries, δa and δA , and their correlations. For unaveraged profiles, the amplitude asymmetry varies in a wide range (± 70 percent) at small amplitudes. The area asymmetry has a similar distribution, but the scatter is smaller. The amplitude asymmetry correlates with the area asymmetry, at positive values they vary in nearly direct proportion. This means that both

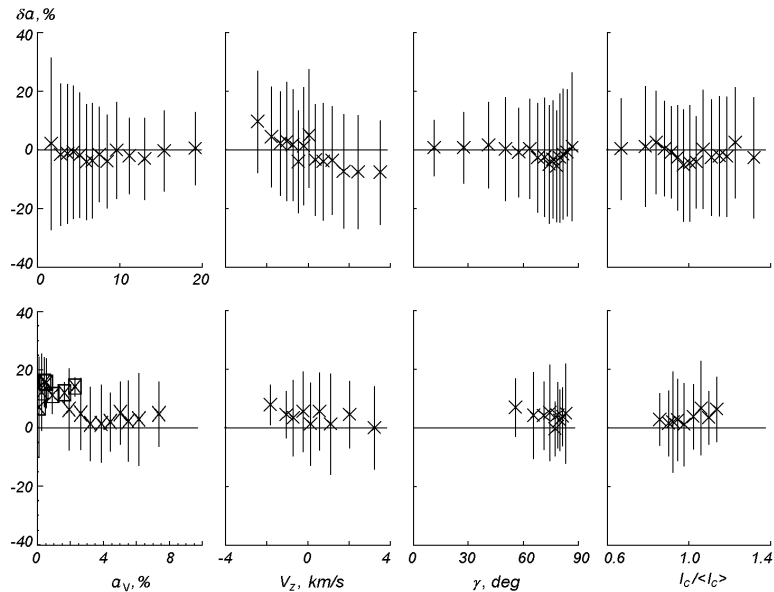


Figure 9: Amplitude asymmetry as a function of mean amplitude of V profile, vertical velocity, field inclination angle, and continuum contrast: upper plots) all profiles, lower plots) profiles averaged with a 700-km step.

asymmetries are caused by the same factors – the velocity field and magnetic field gradients. Mean asymmetries are close to zero ($\overline{\delta a} = -1$, $\overline{\delta A} = 1$ percent for unaveraged profiles and $\overline{\delta a} = 3$, $\overline{\delta A} = -2$ percent for averaged ones). Spatial averaging drastically weakens the correlation between δa and δA and changes the inclination of the relation — the amplitude asymmetry becomes more positive. This suggests that the spatial averaging is also a cause of observed profile asymmetry, the amplitude asymmetry being more sensitive to the averaging. This may be the reason why the amplitude asymmetry measured from observations is greater, as a rule, than the area asymmetry: $\delta a = 15$ percent and $\delta A = 6$ and 4 percent for the Fe I lines $\lambda\lambda$ 630.15 and 630.25 nm [36, 11]. Figure 8 also shows the asymmetries found in FTS observations [47], they are much greater, on the average, than those obtained in our calculations. This discrepancy seems to be caused by a substantial difference in the spatial and temporal averaging and by different activity levels in the observed and simulated regions.

The observed area asymmetry is a factor of 2–3 greater than the amplitude asymmetry. This difference is yet to be explained. Our results suggest that it is caused by insufficient spatial resolution of observations and by atmospheric effects. When the quality of observations and the spatial resolution are upgraded, the relative number of strong V profiles observed in the kilogauss flux tube will increase. Our calculations demonstrate that the asymmetry in such profiles is much smaller because there are no sudden velocity and field strength gradients inside flux tubes as compared to their periphery or the regions of weak turbulence fields of mixed polarity. These properties of strong V profiles also account for a small scatter in their asymmetries, while the scatter for weak V profiles can be as large as 70 percent.

We analyzed the relationship between the V -profile asymmetry and the amplitude a_V , velocity V_z , inclination angle γ , and contrast (Fig. 9). The correlation of δa with these parameters is rather weak; the only feature worthy of notice is an appreciable growth of positive asymmetry with the velocity of upflows while downflows are more often associated with negative amplitude asymmetries.

Center-to-limb variation. Investigations of the center-to-limb variations in the V -profile

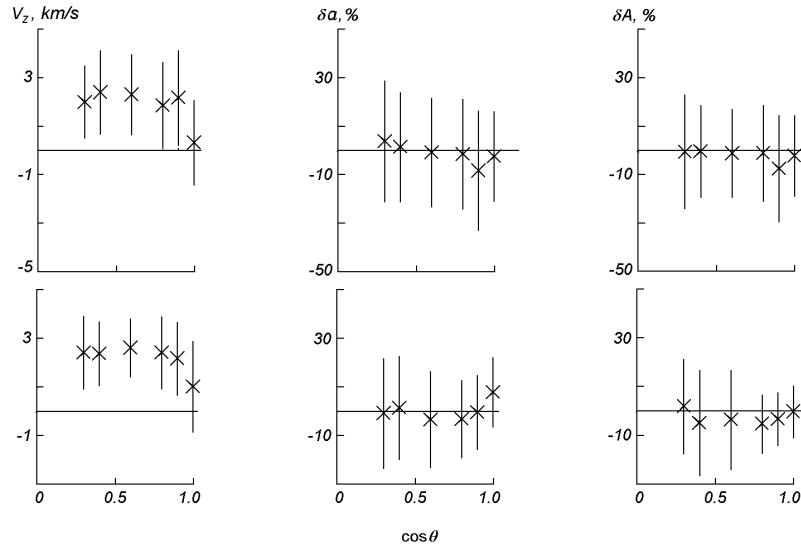


Figure 10: Center-to-limb variations of vertical velocity, amplitude asymmetry, and area asymmetry: upper plots) all profiles, lower plots) profiles averaged with a 700-km step.

shifts and asymmetries involve a huge amount of calculations, and so we selected ten snapshots only. Figure 10 shows the velocity V_z as functions of their position on the disk ($\mu = \cos \theta$). V_z is positive (predominance of downflows) outside the disk center, it amounts up to 2 km s^{-1} , on the average, at $\mu = 0.9$ and changes almost not at all to the limb.

Spatial averaging slightly affects the V_z - μ dependence. According to observations [24], downflows dominate at the disk center, and the profile shifts are close to zero at the limb. Our results can differ from observations for various reasons. We suppose that the velocity increase obtained in our calculations is a result of the canopy effect in the upper parts of flux tubes, where the profiles calculated for $\cos \theta \approx 1$ are formed. According to the 2D MHD simulations used in this paper, the strong flows of matter in the upper layers are predominantly inclined, they are directed slightly downwards, to the centers of intergranular lanes (see Fig. 1). Another reason for the discrepancy can be related to some peculiarities of the 2D MHD models – the upper boundary conditions imposed on the upper layers in the models do not correspond to actual conditions in the upper photosphere. This may affect the calculations of the line profiles far from the disk center, these profiles being formed higher in the photosphere than those which are located closer to the disk center. At the same time the accuracy of observations deteriorates closer to the limb. It should also be noted that there is observational evidence of high horizontal velocities (up to 2 km s^{-1}) [51], and they are in better accord with our results.

The center-to-limb variations of mean asymmetry δa , particularly the asymmetry for averaged profiles, agree satisfactorily with observation data. In FTS observations [49] the amplitude asymmetry diminished from 10–15 percent at the disk center to zero at the limb. In [11] the mean asymmetry δa varied from 15 percent (center) to -5 percent (limb), with the intersection point near $\cos \theta = 0.7$. Similar results were obtained in [24], but δa and δA slightly increased at $\cos \theta = 0.86$ and then monotonically diminished to the limb.

The area asymmetry in our calculations is small and predominantly negative (Fig. 10), while in the FTS observations in [49] the asymmetry is positive at the center, diminishes to the limb and becomes negative. Negative area asymmetries were observed in [24] at the disk center in regions with small filling factor.

One can see in Fig. 10 that the spatial averaging of profiles affected the most the amplitude asymmetry, especially at the disk center. We wish to stress once more that the amplitude asymmetry is the parameter most sensitive to spatial averaging.

6 Conclusion

We used the results of two-dimensional MHD simulation of solar granulation to investigate the motions of matter in magnetic elements with high spatial resolution (35 km). The analysis of the V profiles of the Fe I λ 630.25 nm line synthesized in snapshots of the MHD simulations allowed us to make some inferences as to the vertical velocity of magnetized plasma motions in photospheric regions with a mean magnetic flux density of 0.2 mT and mean unsigned field strength of 35 mT.

1. The mean velocity is 0.5 ± 2 km s⁻¹ with a scatter from -3 to 9 km s⁻¹. Downflows with a mean velocity of 3 ± 2 km s⁻¹ dominate in intergranular regions inside strong vertical flux tubes, while upflows with a mean velocity of 0.5 ± 2 km s⁻¹ are typical of granular regions outside flux tubes.

2. There is a noticeable correlation between the velocity and the amplitude and area asymmetries of V profiles. The positive asymmetry increases, on the average, with upflow velocity. The negative asymmetry occurs most often in the profiles formed at the sites with dominant downflows. The mean asymmetry of amplitudes and areas is about 1 percent with a scatter of 70 percent in weak V profiles and 10 percent in strong ones.

3. The mean velocity fluctuates nonlinearly in time. There are two peaks in the velocity power spectrum — a stronger peak in the 5-min band and a much weaker one in the 3-min band. Velocity fluctuations correlate with gas pressure fluctuations at the surface level, and they also depend on magnetic field fluctuations. The power spectrum of field strength fluctuations has two peaks at periods of 20 and 13 min. Periodic variations of magnetic field strength are related to intensification and dissipation of magnetic fields in strong flux tubes. When the field strength increases, oscillatory downward motions are intensified, and this results in a nonlinearity of mean velocity oscillations.

4. The mean velocity substantially changes when going from the solar disk center to the limb. These changes occur due to intense slopping motions in the upper layers of simulation region. The mean velocity increases to 2 km s⁻¹ at a small distance from the disk center ($\cos\theta = 0.9$), and then it slightly changes to the limb. The amplitude asymmetry decreases and changes its sign from positive to negative when going from the center to the limb of the solar disk. The negative area asymmetry is greater at the limb.

5. The mean velocity depends on spatial averaging of profiles. At lower resolutions the V -profile amplitudes and other parameters substantially change, and they are closer to the observed parameters. The asymmetry of V profiles is the parameter most sensitive to spatial averaging, the amplitude asymmetry growing much faster at lower resolutions than the area asymmetry. This may be a reason why observed amplitude asymmetries are greater than area asymmetries.

Acknowledgements. We wish to thank S. Solanki for the possibility to work at the Max Planck Institute for Aeronomy, for making available FTS observation data, and for useful comments, S. Ploner for his thorough support rendered to the author during her stay at the Max Planck Institute for Aeronomy and for useful discussion, M. Schüssler for discussion of the results, and N. V. Kharchenko for her useful advice on the statistics techniques. We also wish

to thank the referee for useful critical comments. The research described in this publication is a part of an international cooperation program, it was made possible in part by Grant No. CLG97501 from NATO and Grant No. 00084 from INTAS.

References

- [1] M. A. Amer and F. Kneer, “High spatial resolution spectropolarimetry of small-scale magnetic elements on the Sun,” *Astron. and Astrophys.*, vol. 273, no. 1, pp. 304–312, 1993.
- [2] I. N. Atroshchenko and V. A. Sheminova, “Numerical simulation of the interaction between solar granules and small-scale magnetic fields,” *Kinematika i Fizika Nebes. Tel [Kinematics and Physics of Celestial Bodies]*, vol. 12, no. 4, pp. 32–45, 1996.
- [3] I. N. Atroshchenko and V. A. Sheminova, “Simulation of spectral effects with the use of two-dimensional magnetohydrodynamic models of the solar photosphere,” *Kinematika i Fizika Nebes. Tel [Kinematics and Physics of Celestial Bodies]*, no. 5, pp. 32–47, 1996.
- [4] T. E. Berger, C. A. Schrijver, R. A. Shine, et al., “New observations of subarcsecond photospheric bright points,” *Astrophys. J.*, vol. 454, no. 1, pp. 531–544, 1995.
- [5] P. N. Brandt, A. S. Gadun, and V. A. Sheminova, “Absolute shifts of Fe I and Fe II lines in solar active regions (disk center),” *Kinematika i Fizika Nebes. Tel [Kinematics and Physics of Celestial Bodies]*, vol. 13, no.5, pp. 75–86, 1997.
- [6] A. S. Gadun, “Two-dimensional nonstationary magnetogranulation,” *Kinematika i Fizika Nebes. Tel [Kinematics and Physics of Celestial Bodies]*, vol. 16, no. 2, pp. 99–120, 2000.
- [7] A. S. Gadun, V. A. Sheminova, and S. K. Solanki, “Formation of small-scale magnetic elements: surface mechanism,” *Kinematika i Fizika Nebes. Tel [Kinematics and Physics of Celestial Bodies]*, vol. 15, no. 5, pp. 387–397, 1999.
- [8] A. S. Gadun, S. K. Solanki, and A. Johannesson, “Granulation near the solar limb: observations and 2D modelling,” *Astron. and Astrophys.*, vol. 350, no. 3, pp. 1018–1034, 1999.
- [9] A. S. Gadun, S. K. Solanki, V. A. Sheminova, and S. R. O. Ploner, “A formation mechanism of magnetic elements in regions of mixed polarity,” *Solar Phys.*, vol. 203, no. 1, pp. 1–7, 2001.
- [10] S. I. Gopasyuk, V. A. Kotov, A. B. Severny, and T. T. Tsap, “The comparison of the magnetographic magnetic field measured in different spectral lines,” *Solar Phys.*, vol. 31, no. 2, pp. 307–316, 1973.
- [11] U. Grossmann-Doerth, C. U. Keller, and M. Schüssler, “Observations of the quiet Sun’s magnetic field,” *Astron. and Astrophys.*, vol. 315, no. 3, pp. 610–617, 1996.
- [12] U. Grossmann-Doerth, M. Schüssler, and S. K. Solanki, “The effect of non-linear oscillations in magnetic flux tubes of Stokes V asymmetry,” *Astron. and Astrophys.*, vol. 249, no. 1, pp. 239–242, 1991.

- [13] U. Grossmann-Doerth, M. Schüssler, and O. Steiner, “Convective intensification of solar surface magnetic fields: Results of numerical experiments,” *Astron. and Astrophys.*, vol. 337, no. 3, pp. 928–939, 1998.
- [14] E. J. Groth, “Probability distribution related to power spectra,” *Astrophys. J., Suppl. Ser.*, vol. 286, no. 1, pp. 285–302, 1975.
- [15] V. A. Kotov, N. N. Stepanyan, and Z. F. Shcherbakova, “Role of the background magnetic field and the fields of active regions and spots in the general magnetic field of the Sun,” *Izv. Krym. Astrofiz. Observ.*, vol. 56, pp. 75–83, 1977.
- [16] R. Howard and J. O. Stenflo, “On the filamentary nature of solar magnetic fields,” *Solar Phys.*, vol. 22, no. 2, pp. 402–417, 1972.
- [17] C. U. Keller, S. K. Solanki, T. D. Tarbel, et al., “Solar magnetic field strength determinations from high spatial resolution filtergrams,” *Astron. and Astrophys.*, vol. 236, no. 1, pp. 250–255, 1990.
- [18] C. U. Keller, F.-L. Deubner, U. Egger, et al., “On the strength of solar intra-network fields,” *Astron. and Astrophys.*, vol. 286, no. 2, pp. 626–634, 1994.
- [19] E. V. Khomenko, M. Collados, S. K. Solanki, et al., “Quiet-Sun intra-network magnetic fields observed in the infrared,” *Astron. and Astrophys.*, vol. 408, no. 3, pp. 1115–1135, 2003.
- [20] K. D. Leka and O. Steiner, “Understanding small solar magnetic structures: comparing numerical simulations to observation fields,” *Astrophys. J.*, vol. 552, no. 1, pp. 354–371, 2001.
- [21] H. Lin and T. Rimmele, “The granular magnetic fields of the quiet Sun,” *Astrophys. J.*, vol. 514, no. 1, pp. 448–455, 1999.
- [22] B. W. Lites, “Characterization of magnetic flux in the quiet Sun,” *Astrophys. J.*, vol. 573, no. 1, pp. 31–444, 2002.
- [23] B. W. Lites, A. Skumanich, and V. Martinez Pillet, “Vector magnetic fields of emerging solar flux. I. Properties at the solar site of emergence,” *Astron. and Astrophys.*, vol. 333, no. 3, pp. 1053–1068, 1998.
- [24] V. Martinez Pillet, B. W. Lites, and A. Skumanich, “Active region magnetic fields. I. Plage fields,” *Astrophys. J.*, vol. 474, no. 2, pp. 810–842, 1997.
- [25] S. R. O. Ploner, M. Schüssler, S. K. Solanki, and A. S. Gadun, “An example of reconnection and magnetic flux recycling near the solar surface,” in: *Theory, Observation, and Instrumentation*, M. Sigwarth (Editor), *ASP Conf. Ser.*, vol. 236, pp. 363–370, 2001.
- [26] S. R. O. Ploner, M. Schüssler, S. K. Solanki et al., “The formation of one-lobe Stokes V profiles in an inhomogeneous atmosphere,” *ibid.*, pp. 371–378, 2001.
- [27] S. R. O. Ploner, S. K. Solanki, and A. S. Gadun, “The evolution of solar granules deduced from 2D simulations,” *Astron. and Astrophys.*, vol. 352, no. 2, pp. 679–696, 1999.

- [28] D. N. Rachkovskii and T. T. Tsap, “Study of magnetic fields by the method of the ratio of field strengths in lines measured outside active regions on the Sun,” *ibid.*, vol. 71, pp. 79–87, 1985.
- [29] M. Schüssler, “Magneto-convection,” in: *Magnetic Fields Across the Hertzsprung-Russell Diagram*, G. Mathys, S. K. Solanki, and D. T. Wickramasinghe (Editors), ASP Conf. Ser., vol. 258, pp. 115–123, 2001.
- [30] A. B. Severnyi, “On the nature of magnetic fields on the Sun (fine field structure),” *Astron. Zhurn.*, vol. 42, no. 2, pp. 217–232, 1965.
- [31] V. A. Sheminova, *Calculating Stokes Profile Parameters of Magnetic Absorption Lines in Stellar Atmospheres [in Russian]*, Kyiv, 1990 (VINITI File No. 2940-B90, 30 May 1990).
- [32] V. A. Sheminova, “Two-dimensional MHD models of solar magnetogranulation. Testing of models and methods of Stokes diagnostics,” *Kinematika i Fizika Nebes. Tel [Kinematics and Physics of Celestial Bodies]*, vol. 15, no. 5, pp. 398–412, 1999.
- [33] V. A. Sheminova and A. S. Gadun, “Convective shifts of iron lines in the spectrum of the solar photosphere,” *Kinematika i Fizika Nebes. Tel [Kinematics and Physics of Celestial Bodies]*, vol. 18, no. 1, pp. 18–32, 2002.
- [34] V. A. Sheminova, “The Fe I λ 1564.8 nm line and the distribution of solar magnetic fields,” *Kinematika i Fizika Nebes. Tel [Kinematics and Physics of Celestial Bodies]*, vol. 19, no. 2, pp. 107–125, 2003.
- [35] V. A. Sheminova and A. S. Gadun, “Evolution of solar magnetic flux tubes from Stokes parameter observations,” *Astron. Zhurn.*, vol. 77, no. 10, pp. 790–800, 2000.
- [36] M. Sigwarth, K. S. Balasubramaniam, M. Knölker, and W. Schmidt, “Dynamics of solar magnetic elements,” *Astron. and Astrophys.*, vol. 349, no. 3, pp. 941–955, 1999.
- [37] S. K. Solanki, “Stokes V asymmetry and shift of spectral lines,” *Astron. and Astrophys.*, vol. 221, no. 2, pp. 338–341, 1989.
- [38] S. K. Solanki, “Small-scale solar magnetic fields: an overview,” *Space Sci. Rev.*, vol. 31, pp. 1–188, 1993.
- [39] S. K. Solanki, “Small-scale photospheric structure of the solar magnetic fields outside sunspots,” in: *Magnetic Fields Across the Hertzsprung-Russell Diagram*, S. Mathys, S. K. Solanki, and D. T. Wickramasinghe (Editors), ASP Conf. Ser., vol. 258, pp. 45–53, 2001.
- [40] S. K. Solanki and J. O. Stenflo, “Velocities in solar magnetic flux tubes,” *Astron. and Astrophys.*, vol. 170, no. 1–2, pp. 311–329, 1986.
- [41] R. F. Stein and Å. Nordlund, “Simulation of solar granulation. I. General properties,” *Astrophys. J.*, vol. 499, no. 2, pp. 914–933, 1998.
- [42] R. F. Stein and Å. Nordlund, “Solar oscillations and convection. II. Excitation of radial oscillations,” *Astrophys. J.*, vol. 546, no. 1, pp. 585–603, 2001.
- [43] O. Steiner, U. Grossmann-Doerth, M. Knölker, and M. Schüssler, “Dynamical interaction of solar magnetic elements and granular convection: results of a numerical simulation,” *Astrophys. J.*, vol. 495, no. 1, pp. 468–484, 1998.

- [44] J. O. Stenflo, “Magnetic-field structure of the photospheric network,” *Solar Phys.*, vol. 32, no. 1, pp. 41–63, 1973.
- [45] J. A. Stenflo, “A model of the supergranulation network and of active-region plages,” *Solar Phys.*, vol. 4, no. 1, pp. 79–105, 1975.
- [46] J. O. Stenflo and J. W. Harvey, “Dependence of the properties of magnetic fluxtubes on area factor or amount of flux,” *Solar Phys.*, vol. 95, no. 1, pp. 99–118, 1985.
- [47] J. O. Stenflo, J. W. Harvey, J. W. Brault, and S. K. Solanki, “Diagnostics of solar magnetic fluxtubes using a Fourier transform spectrometer,” *Astron. and Astrophys.*, vol. 131, no. 2, pp. 333–346, 1984.
- [48] J. O. Stenflo, C. U. Keller, and A. Candorfer, “Differential Hanle effect and the spatial variation of turbulent magnetic fields on the Sun,” *ibid.*, vol. 329, no. 1, pp. 319–328, 1998.
- [49] J. O. Stenflo, S. K. Solanki, and J. W. Harvey, “Center-to-limb variation of Stokes profiles and the diagnostics of solar magnetic fluxtubes,” *Astron. and Astrophys.*, vol. 171, no. 2, pp. 305–316, 1987.
- [50] T. T. Tsap and I. S. Laba, “Magnetic fields and vertical motions in supergranules,” *Izv. Krym. Astrofiz. Observ.*, vol. 73, pp. 62–70, 1985.
- [51] R. Volmer, F. Kneer, and C. Bendlin, “Short period waves in small-scale magnetic flux tubes on the Sun,” *Astron. and Astrophys.*, vol. 34, no. 1, pp. L1–L4, 1995.
- [52] H. Zirin and R. Cameron, “Properties of the quiet-Sun magnetic fields as revealed by spectrovideomagnetograph,” *Il Nuovo Cimento*, vol. 25C, no. 5–6, pp. 557–563, 2002.